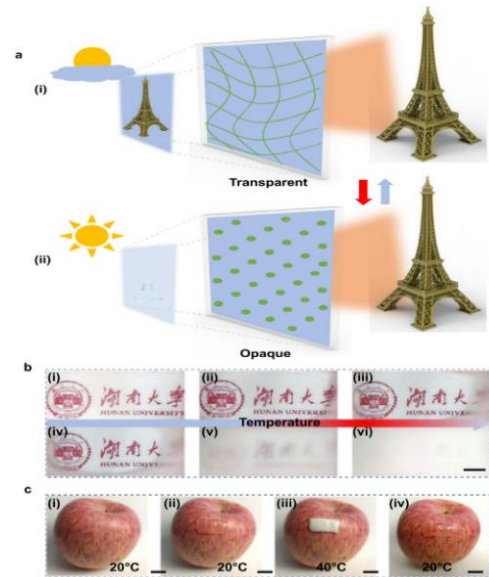


3D printed hydrogel for soft thermo-responsive smart window

Lei Chen, Guihui Duan, Ce Zhang, Ping Cheng and Zhaolong Wang

Highlights:

- A new type of 3D printed hydrogel with amazing flexibility and stretchability(1500%), as well as tunable optical performance controlled by surrounding temperatures is introduced.
- The hydrogel on a PDMS substrate shows transparent-opaque transition with high solar modulation (ΔT_{sol}) up to 79.332% around its lower critical solution temperature (LCST) while maintaining a high luminous transmittance (T_{lum}) of 85.847% at 20°C. It promises great potential applications for the next generation of soft smart windows.
- Selective transparent-opaque transition above LCST can be achieved by patterned hydrogels, which are precisely fabricated via a projection micro-stereolithography based 3D printing technique.



View online: <https://iopscience.iop.org/article/10.1088/2631-7990/ac5ae3>

Article Download: <https://iopscience.iop.org/article/10.1088/2631-7990/ac5ae3/pdf>

Citation: Chen L, Duan G H, Zhang C, Cheng P, Wang Z L. 3D printed hydrogel for soft thermo-responsive smart window. *Int. J. Extrem. Manuf.* 4 025302(2022).

Related articles:

[3D printed ultra-fast photothermal responsive shape memory hydrogel for microrobots](#)

Ziheng Zhan, Lei Chen, Huigao Duan, Yiqin Chen, Min He and Zhaolong Wang

Citation: Zhan Z H, Chen L, Duan H G et al. 3D printed ultra-fast photothermal responsive shape memory hydrogel for microrobots. *Int. J. Extrem. Manuf.* 4 015401(2022).

[Reshapeable, rehealable and recyclable sensor fabricated by direct ink writing of conductive composites based on covalent adaptable network polymers](#)

Xu He, Yuchen Lin, Yuchen Ding, Arif M Abdullah, Zepeng Lei, Yubo Han, Xiaojuan Shi, Wei Zhang and Kai Yu


Citation: He X, Lin Y C, Ding Y C et al. Reshapeable, rehealable and recyclable sensor fabricated by direct ink writing of conductive composites based on covalent adaptable network polymers. *Int. J. Extrem. Manuf.* 4 015302(2022).

[3D printed fiber sockets for plug and play micro-optics](#)

Parvathi S Nair, Jonathan Trisno, Hongtao Wang and Joel K W Yang

Citation: Nair P S, Trisno J, Wang H T, Yang J K W. 3D printed fiber sockets for plug and play micro-optics. *Int. J. Extrem. Manuf.* 3, 015301 (2021).

3D printed hydrogel for soft thermo-responsive smart window

Lei Chen¹, Guihui Duan¹, Ce Zhang², Ping Cheng³ and Zhaolong Wang^{1,*} 

¹ College of Mechanical and Vehicle Engineering, Hunan University, Changsha 410082, People's Republic of China

² Qian Xuesen Laboratory of Space Technology, China Academy of Space Technology (CAST), Beijing 10094, People's Republic of China

³ MOE Key Laboratory for Power Machinery and Engineering, School of Mechanical Engineering, Shanghai Jiao Tong University, Shanghai 200240, People's Republic of China

E-mail: zhaolongwang@hnu.edu.cn

Received 9 September 2021, revised 3 November 2021

Accepted for publication 2 March 2022

Published 25 March 2022



CrossMark

Abstract

Smart windows with tunable optical properties that respond to external environments are being developed to reduce energy consumption in buildings. In the present study, we introduce a new type of 3D printed hydrogel with amazing flexibility and stretchability (as large as 1500%), as well as tunable optical performance controlled by surrounding temperatures. The hydrogel on a PDMS substrate shows transparent-opaque transition with high solar modulation (ΔT_{sol}) up to 79.332% around its lower critical solution temperature (LCST) while maintaining a high luminous transmittance (T_{lum}) of 85.847% at 20 °C. In addition, selective transparent-opaque transition above LCST can be achieved by patterned hydrogels which are precisely fabricated via a projection micro-stereolithography based 3D printing technique. Our hydrogel promises great potential applications for the next generation of soft smart windows.

Supplementary material for this article is available [online](#)

Keywords: 3D printing, thermal response, hydrogel, tunable optical properties, smart window

1. Introduction

Energy dissipation in ventilation, air conditioning, lighting, and heating occupy over 40% of building energy consumption, along with the continuous increase in greenhouse gas emission and global population, greatly worsen the global warming [1, 2]. Thus, smart windows capable of modulating solar radiation in response to the external environment are of great research interests for reducing building energy consumption [3] by tuning light transmittance based on the intensity of sunlight [4–6]. Smart windows are generally fabricated from thermochromic, photochromic, mechanochromic,

and electrochromic materials [4, 7–10]. Among various types of smart windows, thermochromic smart windows are the most widely studied due to their adaptive responses to weather and temperature [11]. The typical vanadium dioxide (VO₂) based thermochromic smart window tailors its solar transmission with a large solar modulation around its critical temperature [12–15]. However, VO₂ based smart windows usually present a high critical temperature and a low luminous transmittance (T_{lum}) with a low solar modulation (ΔT_{sol}), which severely limit its practical applications [11].

Thermal responsive hydrogels have been developed as a new type of thermochromic smart window because their fast, reversible conversion between transparent and opaque states when its temperature exceeds the lower critical solution temperature (LCST) [16]. Thermal responsive hydrogel based windows can achieve the maximum use of heat from sunlight without an external power supply, which plays a significant role in reducing energy consumption [10]. Poly(N-isopropylacrylamide) (PNIPAM) is the most common

* Author to whom any correspondence should be addressed.



Original content from this work may be used under the terms of the [Creative Commons Attribution 3.0 licence](#). Any further distribution of this work must maintain attribution to the author(s) and the title of the work, journal citation and DOI.

thermo-responsive material with a LCST around 32 °C, which is a comfortable temperature for humans [17–19]. PNIPAM based hydrogel exhibits high solar modulation during reversible phase transition around its LCST and a high T_{lum} at room temperature to ensure good indoor visibility, which promises potential for switchable smart windows in practical applications, such as automobiles and buildings [20–22]. However, pure PNIPAM hydrogel exhibits a fragile mechanical property, which is hard for fabricating complex patterns with such a material via traditional manufacturing techniques, limiting its full potential for commercialization. Developing a new kind of hydrogel with excellent mechanical properties, high solar modulation, and high luminous transmittance by new fabrication techniques is in high demand for smart windows [22].

3D printing techniques, also known as additive manufacturing, opens a new gate for the fabrication of complex hydrogel patterns with different desirable properties [23, 24]. With the fast development in 3D printing techniques, various 3D printing methods including stereolithography [25], extrusion 3D printing [26], and digital light processing lithography [27] have been applied to create complex hydrogel patterns due to their merits of design flexibility, low cost, time efficiency, and high precision [28]. Furthermore, printed hydrogels exhibit different unique properties, such as high flexibility [29], large stretchability [30], high conductivity [25], super-anti-freezing [31], self-adhesiveness [32], self-healing [33], etc. Hydrogels with these unique properties are widely applied as sensors [29], human-machine interfaces [31], wearable devices [32], microrobots [17], etc. However, achieving a high-resolution hydrogel pattern acting as smart windows by 3D printing techniques remains challenging due to the lack of stimulus-responsive monomers.

In the present study, we introduced the co-polymerization of N-isopropylacrylamide (NIPAM) and hydrophilic 4-Acryloyl morpholine (ACMO) vinyl monomers to fabricate a thermo-responsive hydrogel achieving sunlight management for designing a smart window. The hydrogel showed high flexibility, tunable mechanical properties, and effective optical properties manipulation. In particular, our hydrogel on a Polydimethylsiloxane (PDMS) substrate was totally transparent in the region of 380–2500 nm with a highest T_{lum} of 85.847% at room temperature. Additionally, our hydrogel presented ultra-fast transparent-opaque transition to modulate solar transmission with a high ΔT_{sol} of 79.332% when the surrounding temperature was above its LCST. Most significantly, our hydrogel was 3D printable with the highest manufacturing resolution up to 40 μm when performed by projection micro-stereolithography (P μ SL) based 3D printing technique. Furthermore, several hydrogel patterns were fabricated to demonstrate our hydrogel's amazing selective transparent-opaque transition, validating its potential applications for energy saving smart windows.

2. Results and discussion

2.1. Hydrogel based soft thermo-responsive smart windows

Figure 1(a) presents the conceptual design of a new type of hydrogel for smart windows controlled by their surrounding

temperature. PNIPAM is the most utilized thermo-responsive polymer with a LCST around 32 °C, while poly (4-Acryloyl morpholine) owns a high LCST at 88 °C because its morpholine is less hydrophobic [34]. The underlying mechanism of thermo-responsive poly(NIPAM-co-ACMO) for light management is that its scattering behavior can be tuned by reversible hydrophilic/hydrophobic phase transitions around its LCST (figure 1(a)). The intermolecular hydrogen bonds between poly(NIPAM-co-ACMO) and water below LCST allow the homogeneous incident light to pass through, which is responsible for a high T_{lum} (figure 1(a-i)). In contrast, the hydrophobic association dominates the transmission of sunlight once the temperature exceeds its LCST, which establishes the optical contrast between poly(NIPAM-co-ACMO) and the surrounding water to strongly scatter the incident light (figure 1(a-ii)). Thereby, the hydrogel changes from a transparent state to an opaque state and blocks the irradiation of scorching sunlight, which is preferable for smart windows.

Figure 1(b) shows the conversion from the transparent state to the opaque state for our printed hydrogel with a thickness of 500 μm . A hydrogel window was colorless and transparent at 20 °C (figure 1(b-i)). Then, the transmittance of our printed hydrogel window decreased with the increase of the temperature (figures 1(b-ii)–(b-v)). Finally, it became translucent and opaque when the temperature reached 40 °C (figure 1(b-vi) and movie S1 (available online at stacks.iop.org/IJEM/4/025302/mmedia)). A hydrogel film was attached to the surface of an apple at different temperatures. Similarly, the hydrogel film was transparent at low temperatures from the comparison of figures 1(c-i) and (c-ii). However, the hydrogel film turned opaque when the temperature exceeded its LCST, and the part of the apple covered by the hydrogel film became invisible (figure 1(c-iii)). The hydrogel film returned to its original transparent state once the temperature decreased to 20 °C, demonstrating its great optical reversibility (figure 1(c-iv)).

2.2. Preparation and printing of the thermo-responsive hydrogel

The photo-curable solution was prepared by mixing specific monomers, a cross-linker, a photoinitiator, and deionized water (tables S1 and S2). ACMO and NIPAM acted as thermo-responsive monomers. Ethyl (2, 4, 6-trimethylbenzoyl) phenylphosphinate (TPO-L) worked as photoinitiator with a relatively high molar attenuation coefficient and efficiency, which initiated the free radical crosslinking co-polymerization of ACMO and NIPAM monomers in the presence of the Poly (ethylene glycol) diacrylate (PEGDA) cross-linker (figure 2(a)). Raman spectroscopy was employed to characterize the 3D printed hydrogel's chemical composition and analyze the presence of poly(NIPAM-co-ACMO) in it (figure 2(b)). The typical Raman signal of CH₃ indicated antisymmetric and symmetric stretching corresponding to the methyl group in the NIPAM monomer and C–O–C stretching in the ACMO monomer, indicating

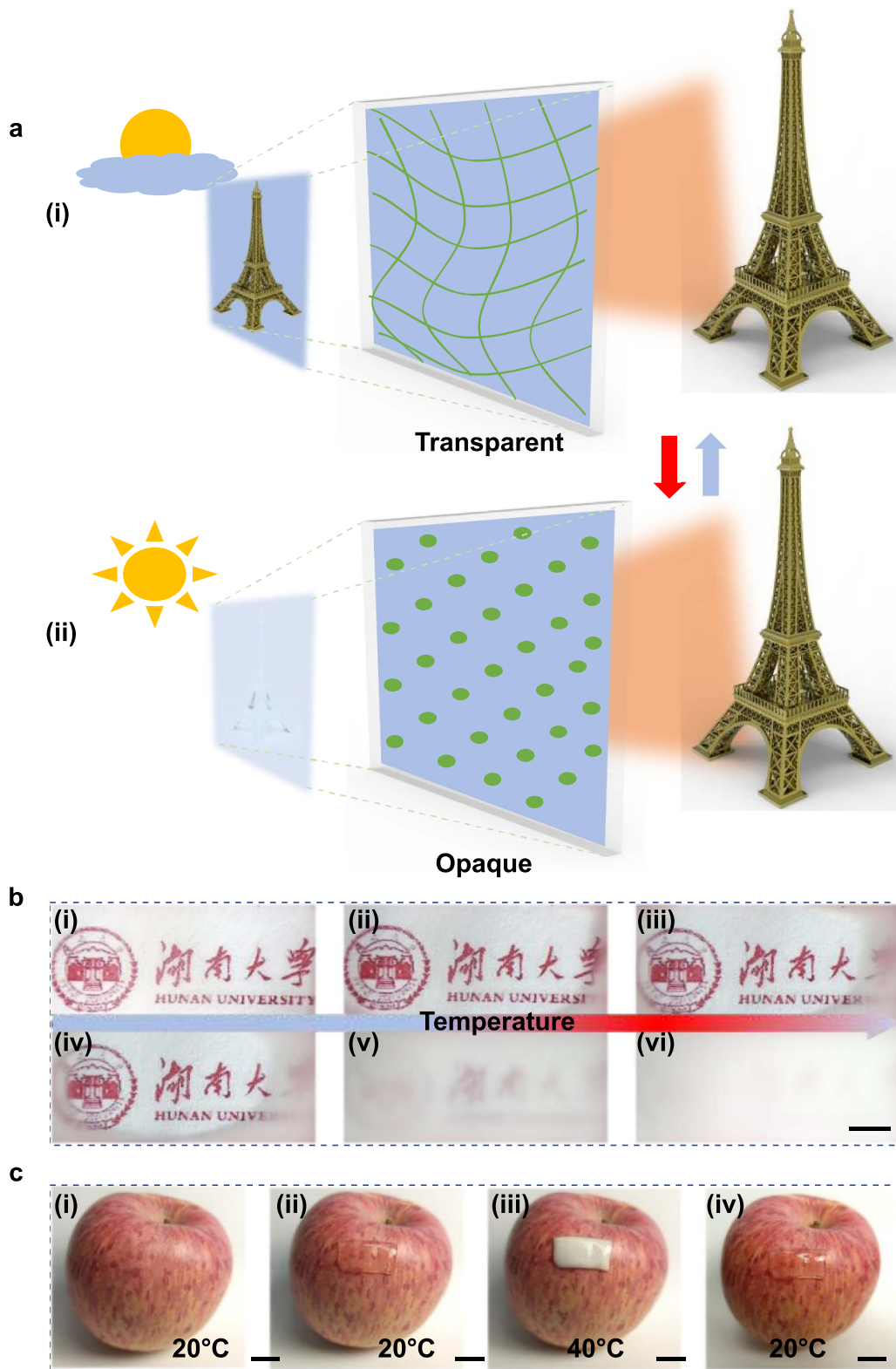


Figure 1. Mechanisms of thermo-responsive hydrogel and conceptual design of our smart window. (a) Schematic of designed optically transparent-opaque switchable window by thermo-responsive hydrogel. (b) Photographs of the thermo-responsive hydrogel window with the increase of the temperature. The scale bar is 5 mm. (c) Photographs of the thermo-responsive hydrogel on the surface of an apple at different temperatures. The scale bar is 10 mm.

the full co-polymerization of anionic NIPAM and ACMO monomers to form the poly(NIPAM -*co*- ACMO) hydrogel network.

Printable hydrogel enables free design and fabrication of various complex patterns. We utilized the P μ SL based 3D printing technique to fabricate hydrogel patterns with

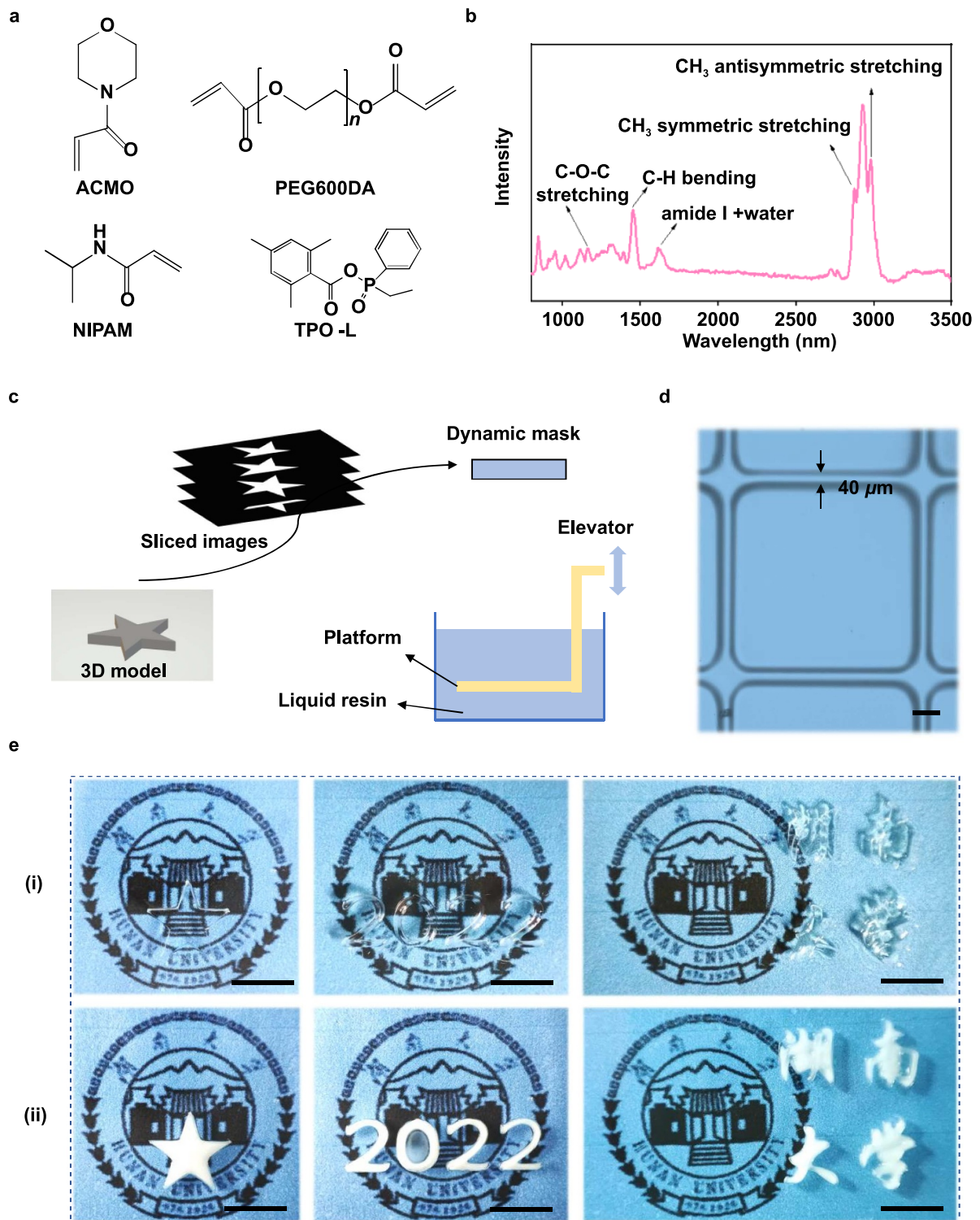


Figure 2. Hydrogel patterns fabricated by $P\mu$ SL based 3D printing technique. (a) Compositions of the photo-curable resin. (b) Raman spectroscopy of the printed hydrogel. (c) Schematic diagrams of $P\mu$ SL based 3D printing technique. (d) A 3D printed high-resolution hydrogel pattern. The scale bar is $100\ \mu\text{m}$. (e) Photographs of selective transparent-opaque transition of patterned hydrogels. The scale bar is 5 mm.

the aforementioned photo-curable solution. As shown in figure 2(c), a designed 3D model was sliced into a series of 2D images, and these 2D images modulated UV light (405 nm) with the corresponding patterns by a digital micromirror device (DMD), which acted as dynamic photo-masks.

The patterned UV light illuminated onto the surface of hydrogel precursor solution to form a solidified structure layer by layer [35]. In order to demonstrate the machinability of our hydrogel, a 2D patterned structure was firstly fabricated (figure 2(d)), indicating the highest printing

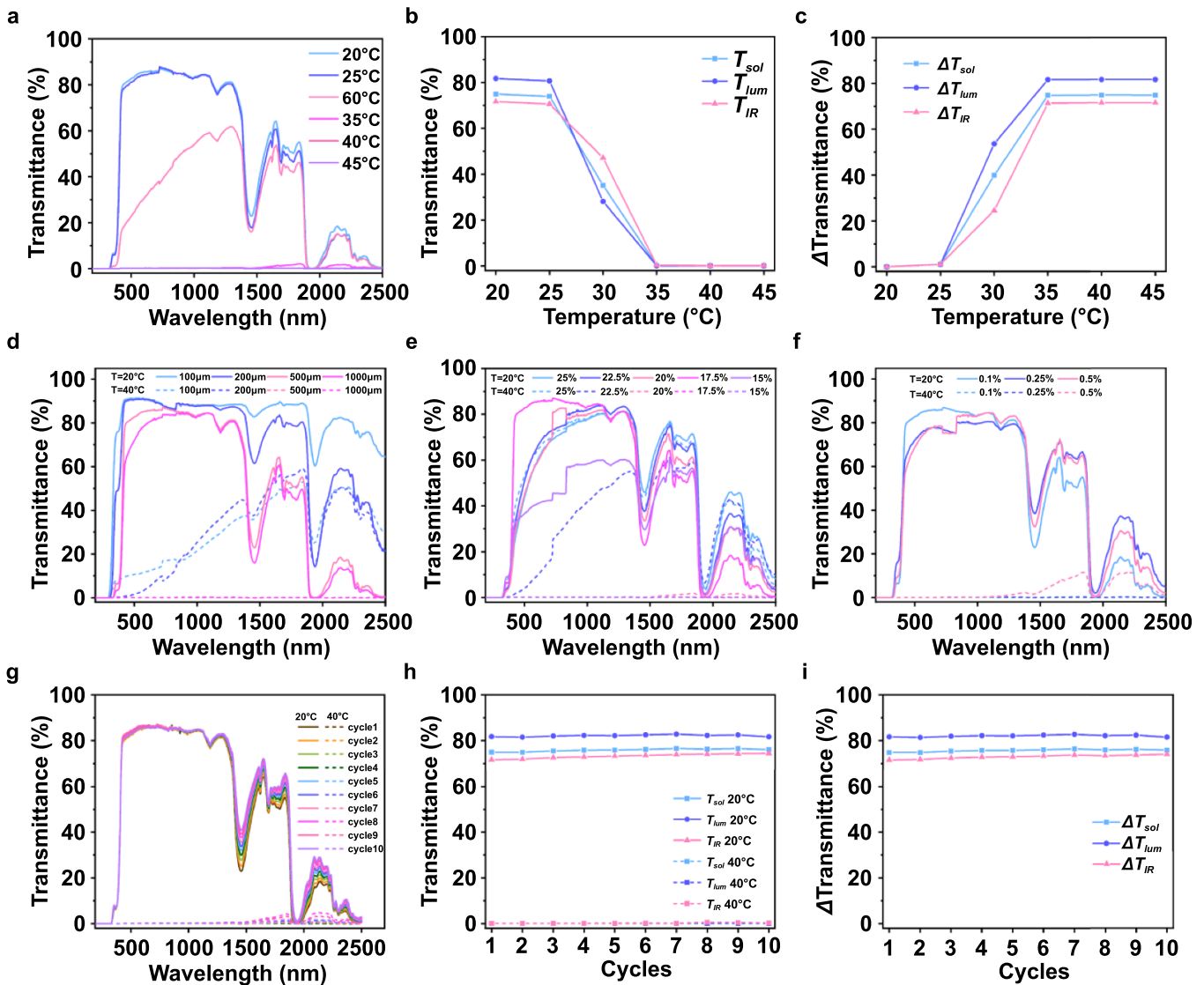


Figure 3. Optical properties of our hydrogel. (a) Transmittance spectra of the hydrogel at different temperatures between 20 °C and 45 °C. (b) T_{lum} , T_{sol} , and T_{IR} of the hydrogel at different temperatures. (c) ΔT_{lum} , ΔT_{sol} , and ΔT_{IR} of the hydrogel at different temperatures. (d) Transmittance spectra of the hydrogel for different thicknesses (100 μm , 200 μm , 500 μm , and 1000 μm) at 20 °C and 40 °C, respectively. (e) Transmittance spectra of a 500 μm hydrogel on a glass substrate for different ACMO contents of 25 wt.%, 22.5 wt.%, 20 wt.%, 17.5 wt.%, and 15 wt.% at 20 °C and 40 °C, respectively. (f) Transmittance spectra of a 500 μm hydrogel on a glass substrate for different PEGDA contents of 0.1 wt.%, 0.25 wt.%, and 0.5 wt.% at 20 °C and 40 °C, respectively. (g) Transmittance spectra of a 500 μm hydrogel on a glass substrate changing the temperature between 20 °C and 40 °C for ten cycles. (h) The stability of T_{lum} , T_{sol} and T_{IR} at 20 °C and 40 °C for ten cycles. (i) The ΔT_{lum} , ΔT_{sol} , and ΔT_{IR} between 20 °C and 40 °C for ten cycles.

resolution up to 40 μm for our hydrogel with P μ SL based 3D printing technique. Next, we fabricated several hydrogel patterns on glass substrates based on the same 3D printing technique. The hydrogel patterns were transparent at 20 °C (figure 2(e-i)). However, the patterned hydrogels presented selective transparent-opaque transition to form shadow when their temperature increased from 20 °C to 40 °C (figures 2(e-ii), S1, and movie S2). The 3D printed complex structures present reversible transparent-opaque transition and high flexibility (figure S1). Such a phenomenon promises significant potential in the field of customized micro-patterned windows and micro-optical switches.

2.3. Transmittance modulation of the thermo-responsive hydrogel window

We further investigated the temperature dependent optical properties of our hydrogel with a thickness of 500 μm on a glass substrate. The optical transmittance spectrum of a glass substrate with a thickness of 1 mm was firstly measured in the region of 380–2500 nm (figure S2). The transmittance of a 500 μm hydrogel film on such a glass substrate within the wavelength range of 200–2500 nm at different temperatures is shown in figure 3(a), and the integral calculation results are summarized in figure 3(b). It can be seen that the transmittance

of the hydrogel window in the visible region (380–780 nm) was higher than 81.758% at 20 °C. When the temperature increased to 40 °C, the hydrogel window converted from the transparent state to opaque state, and its transmittance declined to 0.095%, which exhibited an unprecedented ΔT_{lum} of 81.663% (figure 3(c)). Notably, the T_{sol} decreased sharply from 74.980% to 0.100% when the temperature increased from 20 °C to 40 °C, indicating an extremely high ΔT_{sol} of 74.880% that met the requirements of near-room-temperature transition and sharp gradient of transmittance for an ideal thermochromic smart window.

To further investigate the transparent-opaque transition performance of the hydrogel window, we studied the effect of hydrogel thickness on the optical properties of our printed hydrogel. As can be seen from figure 3(d) and table S3, although a 100 μm hydrogel on a glass substrate demonstrated an impressive T_{lum} of nearly 90%, its high T_{sol} (larger than 18.643% at 40 °C) was unsatisfactory for an ideal smart window. Synchronous trends appeared for both T_{lum} (at 20 °C) and T_{sol} (at 40 °C) to a hydrogel with a thickness of 1000 μm . The extremely high thickness of the hydrogel was accompanied by a relatively low T_{lum} and poor T_{sol} when the temperature was above the LCST. The T_{lum} below the LCST increased with the decreasing thickness of the hydrogel, while the luminous, solar, and IR transmittance ($T_{\text{lum/sol/IR}}$) at temperatures above the LCST increased. A hydrogel with a thickness of 500 μm on a glass substrate was used to investigate the thermo-responsive performance of our hydrogel window with different weight contents of ACMO monomer. The thermo-responsive temperature of a hydrogel window increased with the increasing weight content of ACMO monomer, resulting in a poor modulation of solar radiation within a temperature range from 20 °C to 40 °C (figure 3(e) and table S4). The hydrogel window with a lower content of ACMO monomer presented a much higher $\Delta T_{\text{lum/sol/IR}}$ within a temperature ranging from 20 °C to 40 °C and a relatively lower $T_{\text{lum/sol/IR}}$ at a higher temperature, except for the hydrogel window with 15 wt.% of ACMO who presented a low T_{lum} after UV polymerization at 20 °C.

In addition, the PEGDA cross-linker also played a key role in modulating the luminance transmittance and solar reflectance of our hydrogel window (figure 3(f) and table S5). The T_{lum} and T_{sol} were almost unchanged for hydrogel windows with different weight contents of PEGDA at 40 °C. Whereas T_{lum} and T_{sol} decreased to less than 70.523% and 69.522% at 20 °C, respectively, resulting in the decrease of T_{lum} and T_{sol} with increasing weight content of PEGDA. Moreover, the reusability of our hydrogel window is one of the key points for its practical application. As shown in figure 3(g), the hydrogel window demonstrated little change in light transmittance after varying the temperature between 20 °C and 40 °C for ten cycles. In addition, figures 3(h) and (i) also show that the $T_{\text{lum/sol/IR}}$ at both 20 °C and 40 °C, as well as $\Delta T_{\text{lum/sol/IR}}$ between these two temperatures are respectively constant after ten cycles, indicating that both transmittance and solar modulation abilities of our hydrogel window

are stable and reliable enough acting as a switchable smart window.

2.4. Performance of flexible hydrogel devices

Unlike pure PNIPAM hydrogel based smart windows that present poor mechanical properties, the addition of thermo-responsive ACMO monomer provided the new hydrogel excellent flexibility. As shown in figure 4(a), a hydrogel film on a PDMS substrate exhibited significant flexibility and high transparency at 20 °C with large deformations, such as bending, stretching and twisting, which were fully reversible. Likewise, such a flexible hydrogel device could also endure significant deformation after transitioning from transparent to opaque at 40 °C (figure 4(b)). To further demonstrate the influence of different amounts of ACMO monomer on the mechanical properties of our hydrogels, uniaxial tensile tests were carried out, and the results were shown in figures 4(c) and S3. It could be seen that increasing the weight content of ACMO monomer increased stretchability of the hydrogel before reaching the maximum of 1500% with 20 wt.% ACMO. Then, the stretchability of our hydrogel decreased with the further increase of ACMO. In addition, figures 4(d) and S3 show that increasing the cross-linker concentration decreased stretchability of our printable hydrogel but increased its stress due to a higher crosslinking density and smaller space between polymer chains in the hydrogel films. Moreover, the mechanical property of our hydrogel slightly depended on the temperature. As observed from figures 4(e) and S3, the elongation of the hydrogel slightly decreased from 12.6 to 10.5 when the surrounding temperature increased from 20 °C to 40 °C.

Additionally, the hydrogel could also be printed directly on flexible substrates to produce a flexible thermo-responsive smart window. As shown in figure 4(f) and table S6, a hydrogel film with a thickness of 500 μm was printed on a 500 μm commercial transparent PDMS substrate. It can be seen that the flexible thermo-responsive switchable window exhibited a T_{lum} as high as 85.847%. However, the hydrogel device rapidly became opaque, and the T_{lum} suddenly declined to 0.153% when the temperature increased to 40 °C, which exhibited an extremely high ΔT_{lum} (85.694%). Furthermore, the T_{sol} and T_{IR} decreased significantly from 79.638% to 0.306% and 76.966% to 0.533% at 40 °C, respectively, indicating an extremely high ΔT_{sol} of 79.332% as well as a super-high ΔT_{IR} of 76.433%. Likewise, the hydrogel could also be printed directly on a PC substrate with a thickness of 200 μm , showing high ΔT_{lum} , ΔT_{sol} , and ΔT_{IR} as the temperature increased from 20 °C to 40 °C (figure 4(g)). Figure 4(h) displays a comparison of our work with some previous reported thermochromic counterparts. It can be seen that our flexible hydrogel window presents ultra-high performance in both T_{lum} and ΔT_{sol} when compared with those of previous reported switchable smart windows [12–15, 21, 35–38].

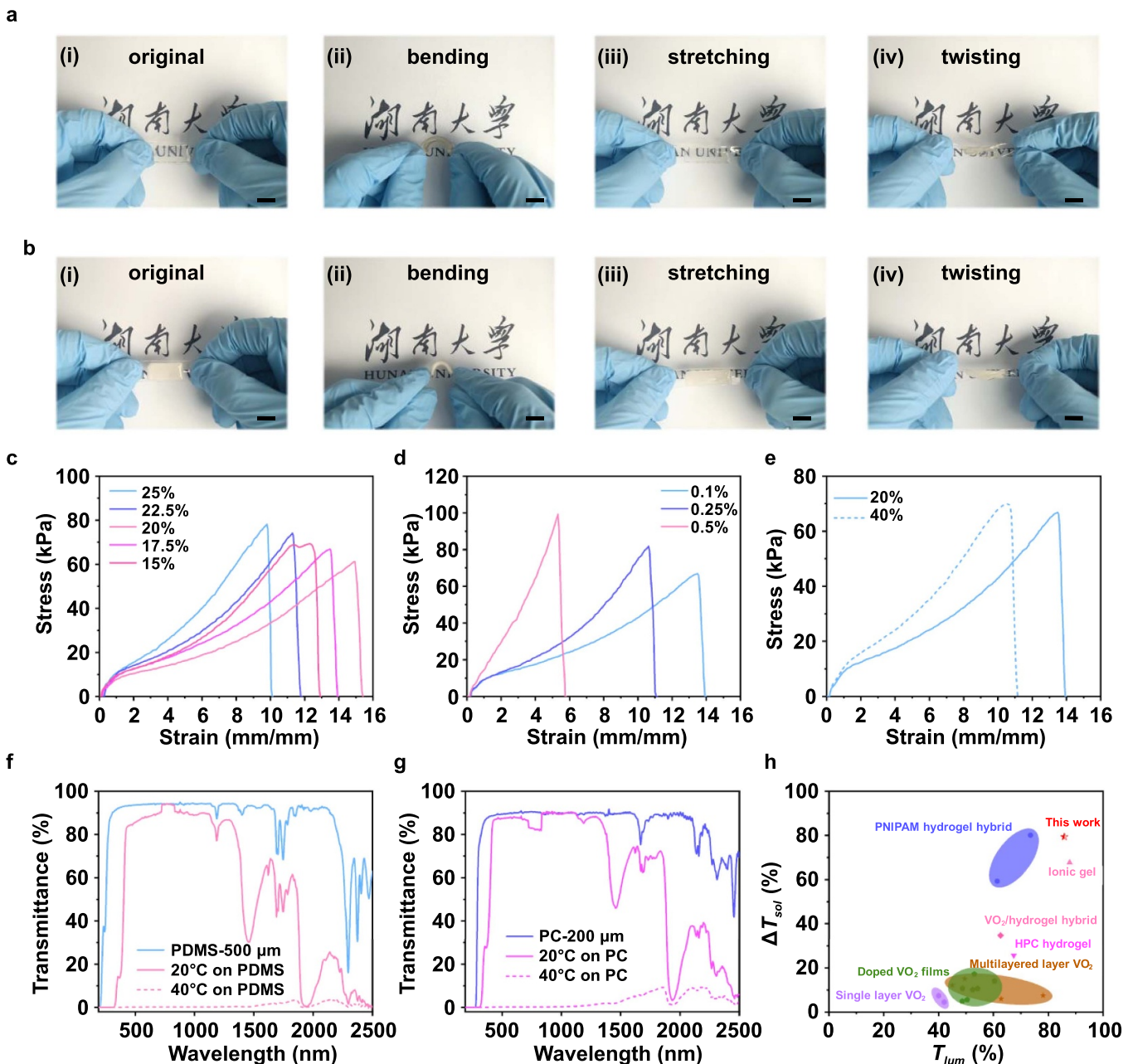


Figure 4. Performance of flexible thermo-responsive hydrogel devices. (a) Photographs of a transparent hydrogel film on PDMS enduring large deformations such as bending, stretching and twisting at 20 °C. The scale bar is 10 mm. (b) Photographs of an opaque hydrogel film on PDMS enabling large deformations such as bending, stretching and twisting at 40 °C. The scale bar is 10 mm. (c) Stress–strain curves of hydrogel with different weight contents of ACMO. (d) Stress–strain curves of hydrogel with different weight contents of PEGDA. (e) Stress–strain curves of hydrogel at different temperatures. (f) Transmittance spectra of a hydrogel film with a thickness of 500 μm on a 500 μm PDMS substrate at 20 °C and 40 °C. (g) Transmittance spectra of a hydrogel film with a thickness of 500 μm on a 200 μm PC substrate at 20 °C and 40 °C. (h) Performance comparisons (T_{lum} and ΔT_{sol}) of our hydrogel window with some previous reported results including singer layer VO_2 [12, 13], multilayered layer VO_2 [12, 13], dope VO_2 films [14, 15], VO_2 /hydrogel hybrid [36], HPC hydrogel [37], ionic gel [38], and PNIPAM hydrogel hybrid [22, 39].

3. Conclusions

We developed a new type of printable hydrogel with excellent flexibility to endure large deformations, such as bending, stretching and twisting, tunable mechanical properties (the largest elongation was 1500%), as well as tunable T_{lum} and T_{sol} via tailoring the material compositions and geometric parameters. The highest printing resolution of our hydrogel

reached up to 40 μm by employing P μ SL based 3D printing technique. Most significantly, the hydrogel film on a PDMS substrate was highly transparent with a T_{lum} as high as 85.847% at 20 °C and exhibited transparent-opaque transition to achieve solar modulation with a large ΔT_{sol} of 79.332% around its LCST. In addition, several hydrogel patterns were fabricated to further present the amazing selective transparent-opaque transition property of our printable hydrogel at a high

temperature. Our printable thermo-responsive hydrogel promises great potential energy-saving applications for the new generation of ideal smart windows.

4. Experimental section

4.1. Materials

4-Acryloylmorpholine (ACMO, Monomer, Chengdu Sicheng Optoelectronic Materials Co., Ltd.), (NIPAM, Monomer, Aladdin), polyethyleneglycol (600) diacrylate (PEG600DA, Cross-linker, RYOJI), (TPO-L, photoinitiator, RYOJI) formed the photo-curable resin. All the materials were used without further purification. Deionized water (18.2 M Ω ·cm) was used throughout all the experiments.

4.2. Preparation of UV curable solution

The UV curable solution was prepared by mixing monomers, cross-linker, photoinitiator, and deionized water. Specifically, 0.2 g TPO-L and 0.02 g PEGDA were dissolved in 3.5 g ACMO monomer using a mechanical stirrer to achieve solution A. Solution B was obtained by dissolving NIPAM (6.5 g) to deionized water (10 ml). After mixing solution A and solution B, the mixture was degassed in the dark for 10 min before being well prepared. For another type of UV curable solution, the weight ratio of ACMO and PEGDA were set as shown in tables S1 and S2.

4.3. P μ SL based 3D printing process

3D printing was performed by a P μ SL printer (S140, BMF, Shenzhen, China) which utilized a UV projector (405 nm) as the light source. The designed 3D structure was firstly sliced into 2D images corresponding to every printing layer by using a software, the patterned UV light was modulated with the corresponding 2D images by using a DMD projector, and then illuminated onto the hydrogel precursor solution to solidify it layer by layer. During the printing process, the printing time was 10 s per layer and the layer thickness was set as 10 μ m.

4.4. Mechanical property test

The mechanical properties of our hydrogels were tested using a mechanical testing apparatus (ZQ-990A, China) with a 20 N load cell. The tensile tests were carried out at 20 °C for hydrogels with different weight contents of ACMO monomer and different concentrations of cross-linker. To investigate temperature dependent mechanical properties of hydrogel, tensile tests were carried out within a temperature range of 20 °C–40 °C. The elongation of the hydrogel was obtained by averaging the results from repeated tests.

4.5. Raman characterization and optical properties measurement

The Raman spectroscopy was measured by a Raman spectrometer (Alpha 300 R, Germany). The transmittance of

hydrogels was performed on a UV-Vis-IR spectrometer (UV-3600Plus, Shimadzu, Japan). The spectrophotometer was equipped with a heating and cooling stage to control the temperature. The integral luminous transmittance T_{lum} (380–780 nm), IR transmittance T_{IR} (780–2500 nm), and solar transmittance T_{sol} (300–2500 nm) are calculated by using the following equations:

$$T_{lum/IR/sol} = \frac{\int \phi_{lum/IR/sol}(\lambda)T(\lambda)d\lambda}{\int \phi_{lum/IR/sol}(\lambda)d\lambda} \quad (1)$$

where $T(\lambda)$ denotes spectral transmittance obtained from a spectrophotometer, $\phi_{lum}(\lambda)$ is the standard luminous efficiency function of photopic vision in the wavelength range of 380–780 nm [19], $\phi_{IR/sol}$ is the IR/solar irradiance spectrum for air mass 1.5 (corresponding to the sun standing 37° above the horizon) [40–45]. According to the data in the tables, part of the measured data is linearly interpolated and then substituted into the formula. $\Delta T_{lum/IR/sol}$ will be obtained by using the equation [22]:

$$\Delta T_{lum/IR/sol} = T_{lum/IR/sol,L} - T_{lum/IR/sol,H} \quad (2)$$

where $T_{lum/IR/sol,L}$ is the integral transmittance at a low temperature and $T_{lum/IR/sol,H}$ is the integral transmittance at a high temperature.

Acknowledgments

LC, GD, and ZW conceived the project, carried out the experimental work, analyzed the data and wrote the manuscript. ZW, PC, and CZ supervised the project. All the authors discussed the results and commented on the manuscript. This work was supported by the National Natural Science Foundation of China (52006056), Key-Area Research and Development Program of Guangdong Province (2020B090923003), Civil Aerospace Technology Research Project (B0108) and Natural Science Foundation of Hunan through Grant No. 2020JJ3012.

ORCID iD

Zhaolong Wang  <https://orcid.org/0000-0003-2967-4546>

References

- [1] Isaac M and van Vuuren D P 2009 Modeling global residential sector energy demand for heating and air conditioning in the context of climate change *Energy Policy* **37** 507–21
- [2] Nakamura C, Yamamoto T, Manabe K, Nakamura T, Einaga Y and Shiratori S 2019 Thermo-responsive, freezing-resistant smart windows with adjustable transition temperature made from hydroxypropyl cellulose and glycerol *Ind. Eng. Chem. Res.* **58** 6424–8
- [3] Aburas M, Soebarto V, Williamson T, Liang R Q, Ebendorff-Heidepriem H and Wu Y P 2019 Thermo-chromic smart window technologies for building application: a review *Appl. Energy* **255** 113522

- [4] Li X H, Liu C, Feng S P and Fang N X 2019 Broadband light management with thermochromic hydrogel microparticles for smart windows *Joule* **3** 290–302
- [5] Wang Z L, Zhang Z M, Quan X J and Cheng P 2018 A numerical study on effects of surrounding medium, material, and geometry of nanoparticles on solar absorption efficiencies *Int. J. Heat Mass Transfer* **116** 825–32
- [6] Wang Z L, Yang P Y, Qi G G, Zhang Z M and Cheng P 2020 An experimental study of a nearly perfect absorber made from a natural hyperbolic material for harvesting solar energy *J. Appl. Phys.* **127** 233102
- [7] Zhou Y, Wang S C, Peng J Q, Tan Y T, Li C C, Boey F Y C and Long Y 2020 Liquid thermo-responsive smart window derived from hydrogel *Joule* **4** 2458–74
- [8] Wang S, Xu Z Q, Wang T T, Xiao T X, Hu X Y, Shen Y Z and Wang L Y 2018 Warm/cool-tone switchable thermochromic material for smart windows by orthogonally integrating properties of pillar[6]arene and ferrocene *Nat. Commun.* **9** 1737
- [9] Ke Y J, Chen J W, Lin G J, Wang S C, Zhou Y, Yin J, Lee P S and Long Y 2019 Smart windows: electro-, thermo-, mechano-, photochromics, and beyond *Adv. Energy Mater.* **9** 1902066
- [10] Kim H N and Yang S 2020 Responsive smart windows from nanoparticle-polymer composites *Adv. Funct. Mater.* **30** 1902597
- [11] Ke Y J, Zhou C Z, Zhou Y, Wang S C, Chan S H and Long Y 2018 Emerging thermal-responsive materials and integrated techniques targeting the energy-efficient smart window application *Adv. Funct. Mater.* **28** 1800113
- [12] Mlyuka N R, Niklasson G A and Granqvist C G 2009 Thermochromic multilayer films of VO₂ and TiO₂ with enhanced transmittance *Sol. Energy Mater. Sol. Cells* **93** 1685–7
- [13] Chen Z, Gao Y F, Kang L T, Du J, Zhang Z T, Luo H J, Miao H Y and Tan G Q 2011 VO₂-based double-layered films for smart windows: optical design, all-solution preparation and improved properties *Sol. Energy Mater. Sol. Cells* **95** 2677–84
- [14] Shen N, Chen S, Chen Z, Liu X L, Cao C X, Dong B R, Luo H J, Liu J J and Gao Y F 2014 The synthesis and performance of Zr-doped and W-Zr-codoped VO₂ nanoparticles and derived flexible foils *J. Mater. Chem. A* **2** 15087–93
- [15] Zhou J D, Gao Y F, Liu X L, Chen Z, Dai L, Cao C X, Luo H J, Kanahira M, Sun C and Yan L M 2013 Mg-doped VO₂ nanoparticles: hydrothermal synthesis, enhanced visible transmittance and decreased metal-insulator transition temperature *Phys. Chem. Chem. Phys.* **15** 7505–11
- [16] Zhou Y, Dong X X, Mi Y Y, Fan F, Xu Q, Zhao H, Wang S C and Long Y 2020 Hydrogel smart windows *J. Mater. Chem. A* **8** 10007–25
- [17] Han D, Lu Z C, Chester S A and Lee H 2018 Micro 3D printing of a temperature-responsive hydrogel using projection micro-stereolithography *Sci. Rep.* **8** 1963
- [18] Tang L, Wang L, Yang X, Feng Y Y, Li Y and Feng W 2021 Poly(N-isopropylacrylamide)-based smart hydrogels: design, properties and applications *Prog. Mater. Sci.* **115** 100702
- [19] Wang L Q, Liu F R, Qian J, Wu Z L and Xiao R 2021 Multi-responsive PNIPAM-PEGDA hydrogel composite *Soft Matter* **17** 10421–7
- [20] Zhu H and Wang L Y 2019 Smart window based on Cu₇S₄/hydrogel composites with fast photothermal response *Sol. Energy Mater. Sol. Cells* **202** 110109
- [21] Wu M C, Shi Y, Li R Y and Wang P 2018 Spectrally selective smart window with high near-infrared light shielding and controllable visible light transmittance *ACS Appl. Mater. Interfaces* **10** 39819–27
- [22] Zhou Y, Layani M, Wang S C, Hu P, Ke Y J, Magdassi S and Long Y 2018 Fully printed flexible smart hybrid hydrogels *Adv. Funct. Mater.* **28** 1705365
- [23] Yin Q, Guo Q, Wang Z L, Chen Y Q, Duan H G and Cheng P 2021 3D-printed bioinspired Cassie–baxter wettability for controllable microdroplet manipulation *ACS Appl. Mater. Interfaces* **13** 1979–87
- [24] Liao Y B, Li W H, Zhan Z H, Duan H G, Liu P, Chen Y Q and Wang Z L 2021 3D-printed complex microstructures with a self-sacrificial structure enabled by grayscale polymerization and ultrasonic treatment *ACS Omega* **6** 18281–8
- [25] Odent J, Wallin T J, Pan W Y, Kruemplestaedter K, Shepherd R F and Giannelis E P 2017 Highly elastic, transparent, and conductive 3D-printed ionic composite hydrogels *Adv. Funct. Mater.* **27** 1701807
- [26] Hong S, Sycks D, Chan H F, Lin S T, Lopez G P, Guilak F, Leong K W and Zhao X H 2015 3D printing of highly stretchable and tough hydrogels into complex, cellularized structures *Adv. Mater.* **27** 4035–40
- [27] Kunwar P, Jannini A V S, Xiong Z, Ransbottom M J, Perkins J S, Henderson J H, Hasenwinkel J M and Soman P 2020 High-resolution 3D printing of stretchable hydrogel structures using optical projection lithography *ACS Appl. Mater. Interfaces* **12** 1640–9
- [28] Li J H, Wu C T, Chu P K and Gelinsky M 2020 3D printing of hydrogels: rational design strategies and emerging biomedical applications *Mater. Sci. Eng. R* **140** 100543
- [29] Ge Q et al 2021 3D printing of highly stretchable hydrogel with diverse UV curable polymers *Sci. Adv.* **7** eaba4261
- [30] Zhang B et al 2018 Highly stretchable hydrogels for UV curing based high-resolution multimaterial 3D printing *J. Mater. Chem. B* **6** 3246–53
- [31] Wang Z L, Chen L, Chen Y Q, Liu P, Duan H G and Cheng P 2020 3D printed ultrastretchable, hyper-antifreezing conductive hydrogel for sensitive motion and electrophysiological signal monitoring *Research* **2020** 1426078
- [32] Chen L, Wang Z L, Zhan Z H, Xie M Z, Duan G H, Cheng P, Chen Y Q and Duan H G 2021 3D printed super-anti-freezing self-adhesive human-machine interface *Mater. Today Phys.* **19** 100404
- [33] Darabi M A, Khosrozadeh A, Mbeleck R, Liu Y Q, Chang Q, Jiang J Z, Cai J, Wang Q, Luo G X and Xing M 2017 Skin-inspired multifunctional autonomic-intrinsic conductive self-healing hydrogels with pressure sensitivity, stretchability, and 3D printability *Adv. Mater.* **29** 1700533
- [34] Kye H, Koh Y G, Kim Y, Han S G, Lee H and Lee W 2017 Tunable temperature response of a thermochromic photonic gel sensor containing N-isopropylacrylamide and 4-acryloylmorpholine *Sensors* **17** 1398
- [35] Ge Q, Li Z Q, Wang Z L, Kowsari K, Zhang W, He X N, Zhou J L and Fang N X 2020 Projection micro stereolithography based 3D printing and its applications *Int. J. Extreme Manuf.* **2** 022004
- [36] Zhou Y, Cai Y F, Hu X and Long Y 2015 VO₂/hydrogel hybrid nanothermochromic material with ultra-high solar modulation and luminous transmission *J. Mater. Chem. A* **3** 1121–6
- [37] Yang Y S, Zhou Y, Yin Chiang F B and Long Y 2016 Temperature-responsive hydroxypropylcellulose based thermochromic material and its smart window application *RSC Adv.* **6** 61449–53
- [38] Lee H Y, Cai Y F, Velioglu S, Mu C Z, Chang C J, Chen Y L, Song Y J, Chew J W and Hu X M 2017 Thermochromic Ionogel: a new class of stimuli responsive materials with super cyclic stability for solar modulation *Chem. Mater.* **29** 6947–55

- [39] Wei G Y, Yang D Y, Zhang T, Yue X J and Qiu F X 2020 Thermal-responsive PNIPAm-acrylic/Ag NRs hybrid hydrogel with atmospheric window full-wavelength thermal management for smart windows *Sol. Energy Mater. Sol. Cells* **206** 110336
- [40] Aden A L and Kerker M 1951 Scattering of electromagnetic waves from two concentric spheres *J. Appl. Phys.* **22** 1242–6
- [41] Wang Z L, Quan X J, Zhang Z M and Cheng P 2018 Optical absorption of carbon-gold core-shell nanoparticles *J. Quant. Spectrosc. Radiat. Transfer* **205** 291–8
- [42] Wang Z L and Cheng P 2019 Enhancements of absorption and photothermal conversion of solar energy enabled by surface plasmon resonances in nanoparticles and metamaterials *Int. J. Heat Mass Transfer* **140** 453–82
- [43] Wang Z L, Zhang Z M, Quan X J and Cheng P 2018 A perfect absorber design using a natural hyperbolic material for harvesting solar energy *Sol. Energy* **159** 329–36
- [44] Liang Q Q, Yin Q, Chen L, Wang Z L and Chen X D 2020 Perfect spectrally selective solar absorber with dielectric filled fishnet tungsten grating for solar energy harvesting *Sol. Energy Mater. Sol. Cells* **215** 110664
- [45] ASTM G159-98 1998 Standard tables for references solar spectral irradiance at air mass 1.5: direct normal and hemispherical for a 37° tilted surface (Withdrawn 2005) (West Conshohocken, PA: ASTM International)